Materials Science-Poland, 39(2), 2021, pp. 265-284
http://www.materialsscience.pwr.wroc.pl/
DOI: 10.2478/msp-2021-0023

Study of load bearing capacity of an infinite sheet weakened by multiple collinear straight cracks with coalesced yield zones

S. Shekhar[1], Naved Akhtar[2,*], S. Hasan[1]

[1]Department of Mathematics, Jamia Millia Islamia, New Delhi 110025, India
[2]Department of Applied Sciences and Humanities, Jamia Millia Islamia, New Delhi 110025, India

This paper is concerned with the analytical solution of a multi-side damage problem. The objective is to investigate the load-bearing capacity of an infinite elastic-plastic plate weakened by three pairs of collinear straight cracks with coalesced yield zones. Stress intensity factors (SIFs) are obtained when yield zones are subjected to three different patterns of yield stress distribution, i. e., constant, linearly, and quadratically varying. Muskhelisvili's complex variable approach is applied for uncovering the solution to this problem. The problem is solved and analyzed rigorously based on Dugdale's hypothesis. The numerical results are deduced for the load-bearing capacity of the plate and yield zone lengths. These results are analyzed and demonstrated graphically for various mechanical loading conditions and different crack lengths.

Keywords: *Multiple collinear cracks, stress intensity factor, Dugdale model, coalesced yield zones, inter-crack distance*

2020 Mathematics Subject Classification (MSC): 74-10, 74A10, 74B05, 74B10.

NOMENCLATURE

$D_i (i = 0,1,2,3)$: Constants of the problem

$F(\theta,k), E(\theta,k), \Pi(\theta,\alpha^2,k)$: Incomplete elliptic integral of first, second, and third kind, respectively

$\pm a_1, \pm b_1, \pm c_1, \pm g_1, \pm g_2$: Physical crack tips

$\pm a, \pm b, \pm c$: Fictitious crack (Extended crack) tips

$L_i (i = 1,2,\ldots,6)$: Crack lengths

$\Gamma_i (i = 1,2,\ldots,9)$: Plastic zones

$z = x + iy$: Complex variable

$P_n(z)$: Polynomial of degree n

$p(t), q(t)$: Applied stresses

Γ': $-\frac{1}{2}(N_1 - N_2)e^{-2i\alpha}$, N_1 and N_2 are the values of principal stresses at infinity, α be the angle between N_1 and the x-axis

$\Omega(z), \Phi(z)$: Complex stress functions

γ: Poisson's ratio

κ: $= \frac{3-\gamma}{1+\gamma}$ for the plane stress. $= 3 - 4\gamma$ for the plane-strain

X_x, Y_y, X_y: Components of stress

σ_{ye}: Yield stress of the plate

σ_∞: Remotely applied stress at the infinite boundary of the plate

1. Introduction

The important task in investigating the fracture or creep nature of engineering structures weakened by cracks or singularities is finding the load-carrying capacity of the structures under various mechanical loading conditions in the presence of a crack. The crack may occur in any structure due to geometrical, environmental, material conditions, and due to the applications of repeated loads.

* E-mail: naved.a86@gmail.com

© 2021. This is an open access article distributed under the Creative Commons Attribution-NonCommercial-NoDerivatives 4.0 License. (http://creativecommons.org/licenses/by-nc-nd/4.0/)

Residual strength of the structures decreases by increasing the length of crack or crack-like defects. Evaluation and analysis of applied load are the main factors for structures containing cracks due to fatigue or stress corrosion cracking. To model such a condition, Dugdale [1] derived a strip yield model to find the strength of a plate containing a single straight crack under uniaxial loading conditions, which play a pioneering role in the development of the field of fracture mechanics. Initially, it was used to solve the only single crack problem under uniform stress distributions, although later it was modified by various researchers, as there is a necessity, for solving different crack configurations, in the presence of various mechanical loading conditions. Some examples are: Harrop [2] modified it to analyze the single crack subjected to quadratically varying yield stresses. Kanninen [3] used Dugdale's method to note the effect of linearly varying tensile stresses on the load-bearing capacity of the plate containing crack. Neimitz [4] discussed Dugdale-Panasyuk model for mode-III moving crack.

Dugdale model is used widely for approximating the plastic zone size due to its mathematical simplicity. Theocaris [5] extended the idea of Dugdale for finding the load-bearing capacity of an infinite plate containing two equal/unequal cracks. Collins et al. [6] used the Dugdale model to analyze the problem of an elastic perfectly plastic plate containing two equal length cracks and also discussed the case of coalesced yield zone between these cracks. Bhargava et al. [7] also used the model to investigate the load-bearing capacity of the plate containing two unequal asymmetrically situated cracks with coalesced yield zones using the complex variable method. Xu et al. [8] applied the weight function approach to solve the problem of two cracks using the Dugdale model. Wu et al. [9] studied the plastic flow of an expanding crack under a uniform in-plane or anti-plane shear stress. The model was further extended to three collinear straight cracks by Hasan et al. [10, 11] and Xu et al. [12]. Dugdale's model also used to evaluate the effect of in-plane constraint, transverse stress, on the fatigue crack closure by Kim et al. [13].

Multiple cracks in a structure develop as non-interacting and being isolated initially. When the length of the crack increases and the space between cracks decreases, a disturbing communication between them starts exponentially that leads to the perturbation in design and finally failure of the structure. Hence, the modelling of the interaction and coalescence yield zones condition between cracks is necessary for the stability of the plate containing multiple interacting cracks. Also, the macroscopic crack developed due to coalescence of two or more microscopic cracks was analyzed by Feng et al. [14]. The complex variable method was used by Bhargava et al. [15] to study the effect of coalescence of yield zones on the load-carrying capacity of the plate containing collinear straight cracks. Akhtar et al. [16] modified Dugdale model to analyze the impact of the coalescence of yield zones between three collinear straight cracks on the bearing capacity of the plate.

Prediction of material behavior in the presence of crack(s) under different mechanical loads causes a serious concern among the engineers who design modern structures. It has been also a challenging task for researchers modeling such a situation or condition mathematically. So many researchers in history visualize the imperativeness of this type of research. It is a harsh reality that finding the exact position of cracks or singularities in a solid is a difficult task. Along with the location of cracks, their size, orientation, coalescence conditions, and interactions between them are also will be the challenging tasks and need to be investigated. Therefore, in this paper, an attempt has been made to study the load-bearing capacity of an infinite elastic perfectly plastic plate weakened by multiple cracks with coalesced yield zones. Here, Dugdale's model has been modified to include the effect of various forms of yield stress distributions. The infinite boundary of the plate is subjected to uniform normal stress distribution. Therefore, cracks are open in mode-I type deformation and yield zones are developed at each crack tip. Moreover, yield zones between each pair of cracks unified due to an increase in the tensile stress acting at the boundary of the plate. Further damage in the plate is seized on the application yield stress distribution within the yield zones and coalesced yield zones. Analytical results

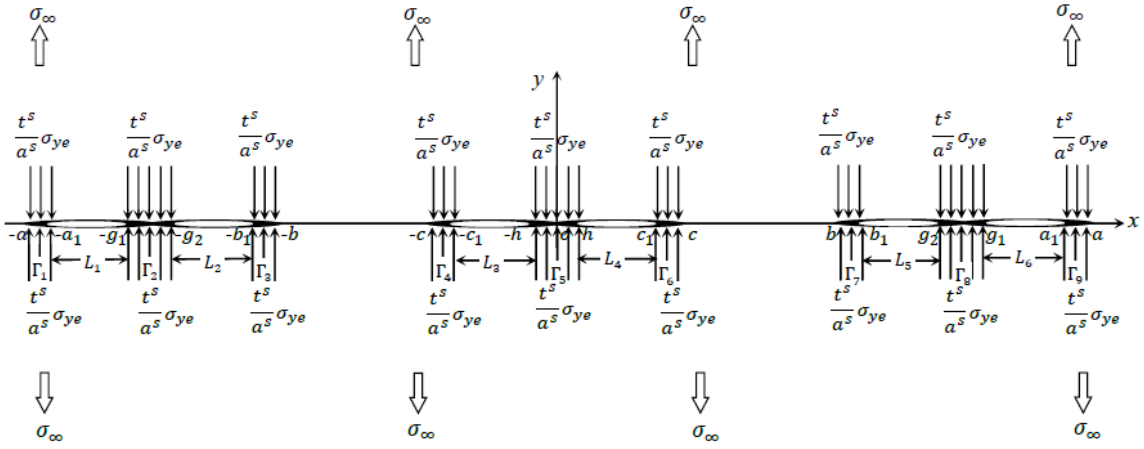


Fig. 1. Configuration of the main problem.

are obtained for important fracture parameters like stress intensity factor, applied load ratio, etc. Numerical results are obtained for applied load ratio in terms of yield zone length, which are reported graphically.

2. The problem under consideration

Consider a multi-site damage problem in which six collinear straight cracks weakening an infinite isotropic elastic-perfectly plastic plate. These cracks are denoted by $L_i (i = 1,2,\ldots,6)$ and occupy the segments $(-a_1,-g_1)$, $(-g_2,-b_1)$, $(-c_1,-h)$, (h,c_1), (b_1,g_2), and (g_1,a_1) on the real x-axis, respectively. Cracks open in mode-I type deformation due to continuous applications of uniform tensile stress distribution σ_∞ at the boundary of the plate which leads to the development of yield zones at each crack tip. Further, the uniform tensile stress σ_∞ increases to such a limit that the yield zones developed between every pair of cracks get coalesced that result in three pairs of collinear straight cracks with coalesced yield zones as given in Figure 1.

These yield zones are denoted by $\Gamma_i (i = 1,2,\ldots,8)$ and occupy the intervals $(-a,-a_1)$, $(-g_1,-g_2)$, $(-b_1,-b)$, $(-c,-c_1)$, $(-h,h)$, (c_1,c), (b,b_1), (g_2,g_1), and (a_1,a), respectively. It is envisaged that the yield zones are subjected to stress distribution $\frac{t^s}{a^s}\sigma_{ye}$ to stop further opening of cracks, where $s = 0,1,2$ denote the constant, linear, and quadratically varying stress distribution and σ_{ye} is the yield stress of the plate.

3. Solution of the problem under consideration

The problem discussed in this section (Section 2) is divided in to two sub-problems, namely *sub-problem A* (opening case) and *sub-problem B* (yielding case) and solved separately. However, depending on the stress distribution acting on the rims of yield zones, three significantly different cases of *sub-problem* B will be considered for $s = 0,1,2$. The solution of the main problem is then obtained by superposing the solution of *Sub-problem A* with each case of *Sub-problem B* one by one. We first discuss the *Sub-problem A* in the Section 3.1. However, the solution of this sub-problem is available already and may be directly taken from [17] and [10].

3.1. Sub-problem A: case of tensile stress distribution

In this section, we discuss the problem of three equal straight cracks weakening an infinite plate as shown in Figure 2. Tensile stress distribution σ_∞ is applied at the boundary of the plate causing the opening of cracks in mode-I type deformation. As a result, yield zones develop at each

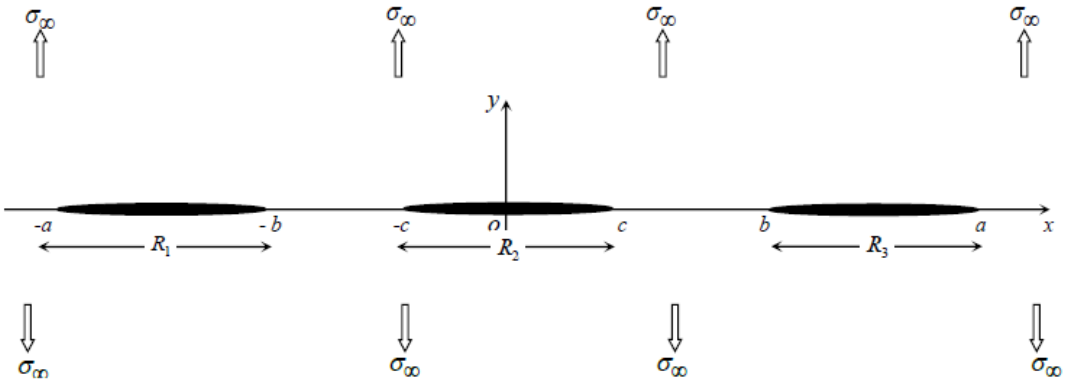


Fig. 2. Configuration of the *Sub-problem A*.

crack tip. The cracks together with the yield zones are treated as fictitious cracks and are denoted by $R_i\,(i=1,2,3)$, and occupy the interval $(-a,-b)$, $(-c,c)$, and (b,a), respectively, as shown in Figure 2.

The mechanical boundary conditions for the problem considered in the section are:

$$Y_y = \sigma_\infty, \quad X_y = 0, \qquad (1)$$
$$when \quad y \to \pm\infty, -\infty < x < \infty$$

$$Y_y = X_y = 0, \quad when \quad y = 0, x \in \bigcup_{i=1}^{3} R_i, \qquad (2)$$

which implies boundary of the sheet is subjected to uniform tensile stresses in absence of body forces.

The complex potential function $\Phi_A(z)$ for this case may be obtained using Eqs. (39, 40) under the boundary conditions (1–2),

$$\Phi_A(z) = \qquad (3)$$
$$\frac{\sigma_\infty}{2}\left[\frac{1}{\chi(z)}\left\{z^3 - z\left(c^2 + \left(a^2 - c^2\right)\lambda^2\right)\right\} - \frac{1}{2}\right],$$

where, subscript A denotes that the function is related to *sub-problem A*,

$$\chi(z) = \sqrt{\left(z^2-a^2\right)\left(z^2-b^2\right)\left(z^2-c^2\right)},$$
$$\lambda^2 = \frac{E(k)}{F(k)}; \quad k^2 = \frac{a^2-b^2}{a^2-c^2}$$

and $F(k)$ and $E(k)$ are complete elliptical integrals of first and second kind, respectively, as given in [18].

Now, with the help of Eq. (3) we can easily obtain the opening mode (mode-I) stress intensity factor at each crack tip by substituting $\Phi_A(z)$ into Eq. (44). After taking corresponding limits, the closed-form expressions of SIFs at extended crack tips a, b, and c are obtained and may be written as:

$$K_A^a = \sigma_\infty\left(1-\lambda^2\right)\sqrt{\frac{\pi a}{k}}, \qquad (4)$$

$$K_A^b = \sigma_\infty\left(\frac{\lambda^2}{1-k^2} - 1\right)\frac{\sqrt{\pi b\left(1-k^2\right)}}{k}, \qquad (5)$$

$$K_A^c = \sigma_\infty\frac{\sqrt{\pi c}}{\sqrt{1-k^2}}\lambda^2, \qquad (6)$$

respectively. Here, superscripts a, b, and c denote the stress intensity factor related to respective crack tip.

3.2. Sub-problem B. For yield stress distribution

In the present section, we will be discussing the case of six straight collinear cracks with coalesced yield zones when faces of the yield zones are subject to yield stress distribution. Since, three different profiles of the yield stress of the form $\frac{t^s}{a^s}\sigma_{ye}; (s=0,1,2)$ are assumed to be acted on the developed yield zones, three different cases of *sub-problem B* will be discussed in this section.

- Case-1: When $s=0$, general yielding conditions (as shown in Figure 3)

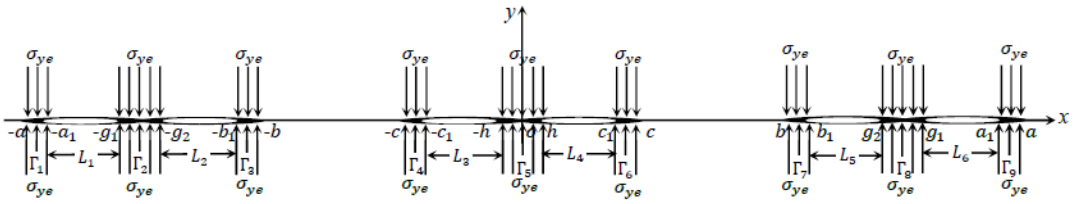


Fig. 3. Configuration of the *Sub-problem B* (when $s = 0$).

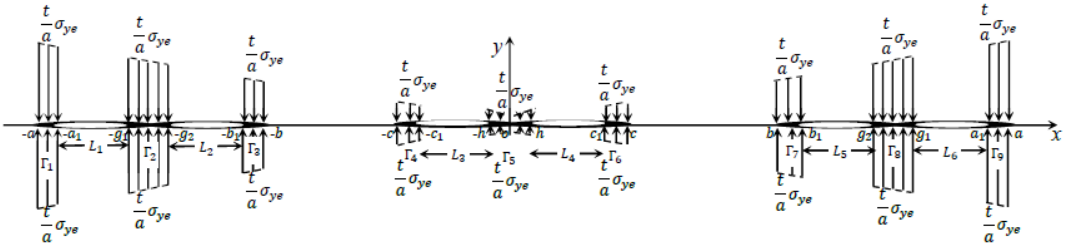


Fig. 4. Configuration of the *Sub-problem B* (when $s = 1$).

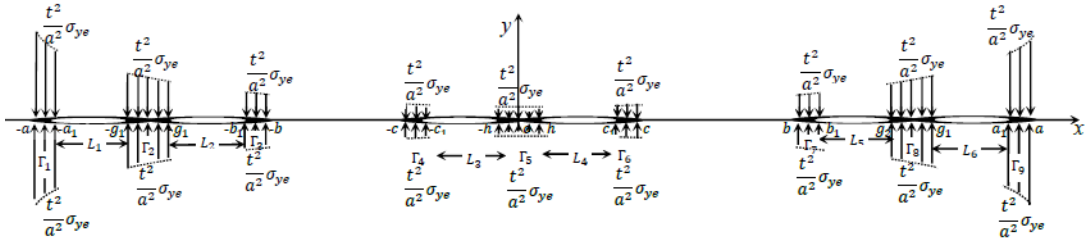


Fig. 5. Configuration of the *Sub-problem B* (when $s = 2$).

- Case-2: When $s = 1$, linearly varying yield stress distribution (as shown in Figure 4)
- Case-3: When $s = 2$, quadratically varying yield stress distribution (as shown in Figure 5)

Case-1: deals with the situation when the yield zones are assumed to be subjected to yield stress distribution to arrest the opening of cracks at each tip. Some structures may fail at a stress level that is well below the yield stress of the material [19], therefore a linearly varying yield stress distribution is assumed on the rims of yield zones in case-2.

Furthermore, in case-3 a quadratically varying stress distribution is assumed to be acted on the faces of yield zones in order to study the situation discussed in case-2 more effectively.

The combined boundary conditions for all three cases for the *sub-problem B* are given below. However, by putting the value $s = 0, 1, 2$ we can use these boundary conditions for three different cases separately:

$$Y_y = 0, \quad X_y = 0, \qquad (7)$$
$$\text{when} \quad y \to \pm\infty, -\infty < x < \infty$$

$$Y_y = \frac{t^s}{a^s}\sigma_{ye}, \quad X_y = 0, \qquad (8)$$
$$\text{when} \quad y \to 0, x \in \bigcup_{n=1}^{9} \Gamma_n$$

These boundary conditions indicate that infinite boundary of the plate is stress free and the faces of yield zones are subjected to the yield stress distribution of the form $Y_y = \frac{t^s}{a^s}\sigma_{ye}$.

On solving the Eqs. (39, 40) under the boundary conditions (7, 8), one can write the complex potential function for the *sub-problem B* as written below

$$\Phi_{B(s)}(z) = \frac{\sigma_{ye}}{2\pi i \chi(z)}\left[\int_{L'} \frac{t^s \chi(t)\,dt}{a^s(t-z)} + i\left(D_{1(s)}z^2 + D_{2(s)}z + D_{3(s)}\right)\right], \quad \{s = 0,1,2\}, \tag{9}$$

Where,

$$L' = [-a,-a_1]\cup[-g_1,-g_2]\cup[-b_1,-b] \cup[-c,-c_1]\cup[-h,h]\cup[c_1,c] \cup[b,b_1]\cup[g_2,g_1]\cup[a_1,a],$$

subscript B indicates the case of *sub-problem B*. Subscript in bracket (s) represent the stress profiles under consideration.

The integral appeared in Eq. (9) is evaluated by using the following forms of $\chi(t)$:

$$\chi(t) = \chi(-t) = i\sqrt{a^2-t^2}\sqrt{t^2-b^2}\sqrt{t^2-c^2}, \quad \text{when} \quad -a < t < -b \text{ or } b < t < a, \tag{10}$$

$$\chi(t) = \chi(-t) = -i\sqrt{a^2-t^2}\sqrt{b^2-t^2}\sqrt{c^2-t^2}, \quad \text{when} \quad -c < t < c, \tag{11}$$

Hence, after a long and complicated mathematical calculation the integral takes the form

$$\begin{aligned}\frac{1}{2}\int_{L'} \frac{t^s\chi(t)}{t-z}dt &= z\left[\int_{a_1}^{a} \frac{t^s\chi(t)}{t^2-z^2}dt + \int_{b}^{b_1} \frac{t^s\chi(t)}{t^2-z^2}dt + \int_{d_1}^{d_2} \frac{t^s\chi(t)}{t^2-z^2}dt + \int_{c_1}^{c} \frac{t^s\chi(t)}{t^2-z^2}dt\right] \\ &= 2iza^{s+2}\left[\frac{m^3}{k}\left\{I_{1(2s+1)} + \left(1-\frac{1}{n^2(z)}\right)H_{1(2s+1)}(z)\right\}\right. \\ &\quad \left. -\frac{m_2^{s+1}}{k_2}\left\{I_{2(2s+2)} + \left(1-\frac{1}{n_2^2(z)}\right)H_{2(2s+2)}(z)\right\}\right],\end{aligned} \tag{12}$$

*All the terms used here are given in Appendix B.

The constants $D_{1(s)}$ and $D_{3(s)}$ vanish due to symmetrical mechanical loading conditions. On the other side, constant $D_{2(s)}$ (for each stress profile) be obtained using the condition of single-value given in Eq. (41), thus, [1]

$$D_{2(0)} = -\frac{2am}{k}\begin{bmatrix} am^2\left(J_{11}-\lambda^2 J_{12}\right) \\ +c_1\tau(\psi(c_1),k) \\ -h\tau(\psi(h),k) \\ +\nu_1-\nu_2+\lambda^2\nu_3 \end{bmatrix}, \tag{13}$$

$$D_{2(1)} = -\frac{2m}{k}\begin{bmatrix} a^2m^2\left(J_{13}-\lambda^2 J_{14}\right) \\ +\frac{c_1^2}{2}\tau(\psi(c_1),k) \\ -\frac{h^2}{2}\tau(\psi(h),k) \\ +W_6-W_7+\frac{\lambda^2}{2}W_8 \end{bmatrix}, \tag{14}$$

$$D_{2(2)} = -\frac{2m}{ak}\begin{bmatrix} a^3m^2\left(J_{15}-\lambda^2 J_{16}\right) \\ +\frac{c_1^3}{3}\tau(\psi(c_1),k) \\ -\frac{h^3}{3}\tau(\psi(h),k) \\ +b^2\left(\nu_1-\frac{\nu_2}{3}\right)+\frac{a^2\lambda^2}{3}\nu_3 \\ -\nu_4+\left(1-k^2-\lambda^2\right)\frac{\nu_5}{3} \end{bmatrix}, \tag{15}$$

Hence, the final form of the complex potential function $\Phi_B(z)$ for the *sub-problem B* may be obtained by substituting Eqs. (12–15) into Eq. (9),

$$\Phi_{B(s)}(z) = \frac{za^2\sigma_{ye}}{\pi\chi(z)}\begin{bmatrix} \frac{m^3}{k}\left\{I_{1(2s+1)}+\left(1-\frac{1}{n^2(z)}\right)H_{1(2s+1)}(z)\right\} \\ -\frac{m_2^{s+1}}{k_2}\left\{I_{2(2s+2)}+\left(1-\frac{1}{n_2^2(z)}\right)H_{2(2s+2)}(z)\right\} \\ +\frac{D_{2(s)}}{2a^2} \end{bmatrix}, \tag{16}$$

[1] All the unknown terms are defined in Appendix B

The opening mode stress intensity factors (SIFs) for the *Sub problem B* at each crack tips a,b, and c are then determined by using Eqs. (16) and (44) for yield stress distribution ($s=0$)

$$K^a_{B(0)} = \frac{2a^3\sigma_{ye}}{\sqrt{a\pi}\sqrt{a^2-b^2}\sqrt{a^2-c^2}}\left(\frac{D_{2(0)}}{2a^2} + \frac{m^3}{k}\left(I_{1(1)} - H_{1(1)}(a)\right) - \frac{m_2}{k_2}\left\{I_{2(2)} + \left(1-\frac{1}{m_2^2}\right)H_{2(2)}(a)\right\}\right), \quad (17)$$

$$K^b_{B(0)} = \frac{-2a^2b\sigma_{ye}}{\sqrt{b\pi}\sqrt{a^2-b^2}\sqrt{b^2-c^2}}\left(\frac{m^3}{k}I_{1(1)} + \frac{D_{2(0)}}{2a^2} - \frac{m_2}{k_2}\left\{I_{2(2)} + \left(1-\frac{1}{k_2^2}\right)H_{2(2)}(b)\right\}\right), \quad (18)$$

$$K^c_{B(0)} = \frac{-2a^2c\sigma_{ye}}{\sqrt{c\pi}\sqrt{b^2-c^2}\sqrt{a^2-c^2}}\left(-\frac{m_2}{k_2}I_{2(2)} + \frac{D_{2(0)}}{2a^2} + \frac{m^3}{k}\left\{I_{1(1)} + \left(1-\frac{1}{k^2}\right)H_{1(1)}(c)\right\}\right), \quad (19)$$

For linearly varying stress distribution ($s=1$) at each crack tips a,b, and c

$$K^a_{B(1)} = \frac{2a^3\sigma_{ye}}{\sqrt{a\pi}\sqrt{a^2-b^2}\sqrt{a^2-c^2}}\left(\frac{D_{2(1)}}{2a^2} + \frac{m^3}{k}\left(I_{1(3)} + H_{1(3)}(a)\right) - \frac{m_2^2}{k_2}\left\{I_{2(4)} + \left(1-\frac{1}{m_2^2}\right)H_{2(4)}(a)\right\}\right), \quad (20)$$

$$K^b_{B(1)} = \frac{-2a^2b\sigma_{ye}}{\sqrt{b\pi}\sqrt{a^2-b^2}\sqrt{b^2-c^2}}\left(\frac{m^3}{k}I_{1(3)} + \frac{D_{2(1)}}{2a^2} - \frac{m_2^2}{k_2}\left\{I_{2(4)} + \left(1-\frac{1}{k_2^2}\right)H_{2(4)}(b)\right\}\right), \quad (21)$$

$$K^c_{B(1)} = \frac{-2a^2c\sigma_{ye}}{\sqrt{c\pi}\sqrt{b^2-c^2}\sqrt{a^2-c^2}}\left(\frac{D_{2(1)}}{2a^2} - \frac{m_2^2}{k_2}I_{2(4)} + \frac{m^3}{k}\left\{I_{1(3)} + \left(1-\frac{1}{k^2}\right)H_{1(3)}(c)\right\}\right), \quad (22)$$

For quadratically varying stress distribution ($s=2$) at each crack tips a,b, and c

$$K^a_{B(2)} = \frac{2a^3\sigma_{ye}}{\sqrt{a\pi}\sqrt{a^2-b^2}\sqrt{a^2-c^2}}\left(\frac{D_{2(2)}}{2a^2} + \frac{m^3}{k}\left(I_{1(5)} + H_{15}(a)\right) - \frac{m_2^3}{k_2}\left\{I_{2(6)} + \left(1-\frac{1}{m_2^2}\right)H_{2(6)}(a)\right\}\right), \quad (23)$$

$$K^b_{B(2)} = \frac{-2a^2b\sigma_{ye}}{\sqrt{b\pi}\sqrt{a^2-b^2}\sqrt{b^2-c^2}}\left(\frac{m^3}{k}I_{1(5)} + \frac{D_{2(2)}}{2a^2} - \frac{m_2^3}{k_2}\left\{I_{2(6)} + \left(1-\frac{1}{k_2^2}\right)H_{2(6)}(b)\right\}\right), \quad (24)$$

$$K^c_{B(2)} = \frac{-2a^2c\sigma_{ye}}{\sqrt{c\pi}\sqrt{b^2-c^2}\sqrt{a^2-c^2}}\left(\frac{m^3}{k}\left\{I_{1(5)} + \left(1-\frac{1}{k^2}\right)H_{1(5)}(c)\right\} - \frac{m_2^3}{k_2}I_{2(6)} + \frac{D_{2(2)}}{2a^2}\right). \quad (25)$$

where $K^t_{B(s)}$ denotes the stress intensity factor at the crack tip t for stress profile s and *sub-problem B*.

4. Applications

In this section, the relation between yield zones lengths, $|a-a_1|, |b_1-b|, |c-c_1|$ and applied load ratio $\left(\frac{\sigma_\infty}{\sigma_{ye}}\right)$ at each crack tips a,b, and c is determined. By the principle of superposition, three

non-linear equations for each stress profile are obtained by equating the corresponding SIFs at each crack tip. This enables to determine a relation between yield zone length and applied load ratio using Eqs. (4–6) and (17–25).

4.1. Yield zone length due to yield stress distribution (Figure 3)

On equating the SIFs K_A^a, K_A^b, and K_A^c from Eqs. (4–6) with $K_{B(0)}^t, (t = a,b,c)$ from Eqs. (17–19) respectively, we get three non-linear equations at each crack tip $t = a,b,c$

$$\frac{m^2}{k^2}\left(1-\lambda^2\right)\left(\frac{\sigma_\infty}{\sigma_{ye}}\right)_{a(0)} + \frac{2}{\pi}\left[\frac{m^3}{k}\left(I_{1(1)}-I_{1(2)}\right) - \frac{m_2}{k_2}\left\{I_{2(2)} + \left(1-\frac{1}{m_2^2}\right)H_{2(2)}(a)\right\} + \frac{D_{2(0)}}{2a^2}\right] = 0, \tag{26}$$

$$\frac{m^2}{k^2}\left(1-k^2-\lambda^2\right)\left(\frac{\sigma_\infty}{\sigma_{ye}}\right)_{b(0)} + \frac{2}{\pi}\left[\frac{m^3}{k}I_{1(1)} - \frac{m_2}{k_2}\left\{I_{2(2)} + \left(1-\frac{1}{k_2^2}\right)H_{2(2)}(b)\right\} + \frac{D_{2(0)}}{2a^2}\right] = 0, \tag{27}$$

$$\frac{m^2}{k^2}\lambda^2\left(\frac{\sigma_\infty}{\sigma_{ye}}\right)_{c(0)} - \frac{2}{\pi}\left[\frac{m^3}{k}\left\{I_{1(1)} + \left(1-\frac{1}{k^2}\right)H_{1(1)}(c)\right\} - \frac{m_2}{k_2}I_{2(2)} + \frac{D_{2(0)}}{2a^2}\right] = 0. \tag{28}$$

4.2. Yield zone length under linearly varying yield stress distribution (Figure 4)

Further, on superposing the solutions in case of linearly varying stress distribution, we get the following equations by using Eqs. (4–6) and (20–22)

$$\frac{m^2}{k^2}\left(1-\lambda^2\right)\left(\frac{\sigma_\infty}{\sigma_{ye}}\right)_{a(1)} + \frac{2}{\pi}\left\{\frac{m^3}{k}\left(I_{1(3)}+H_{1(3)}(a)\right) - \frac{m_2^2}{k_2}\left\{I_{2(4)} + \left(1-\frac{1}{m_2^2}\right)H_{2(4)}(a)\right\} + \frac{D_{2(1)}}{2a^2}\right\} = 0, \tag{29}$$

$$\frac{m^2}{k^2}\left(1-k^2-\lambda^2\right)\left(\frac{\sigma_\infty}{\sigma_{ye}}\right)_{b(1)} + \frac{2}{\pi}\left\{\frac{m^3}{k}I_{1(3)} - \frac{m_2^2}{k_2}\left\{I_{2(4)} + \left(1-\frac{1}{k_2^2}\right)H_{2(4)}(b)\right\} + \frac{D_{2(1)}}{2a^2}\right\} = 0, \tag{30}$$

$$\frac{m^2}{k^2}\lambda^2\left(\frac{\sigma_\infty}{\sigma_{ye}}\right)_{c(1)} - \frac{2}{\pi}\left\{\frac{m^3}{k}\left\{I_{1(3)} + \left(1-\frac{1}{k^2}\right)H_{1(3)}(c)\right\} - \frac{m_2^2}{k_2}I_{2(4)} + \frac{D_{2(1)}}{2a^2}\right\} = 0. \tag{31}$$

4.3. Yield zone length under quadratically varying yield stress distribution (Figure 5)

Furthermore, Eqs. (4, 23), (5, 24), and (6, 25) yields

$$\frac{m^2}{k^2}\left(1-\lambda^2\right)\left(\frac{\sigma_\infty}{\sigma_{ye}}\right)_{a(2)} + \frac{2}{\pi}\left\{\frac{m^3}{k}\left(I_{1(5)}+H_{1(5)}(a)\right) - \frac{m_2^3}{k_2}\left\{I_{2(6)} + \left(1-\frac{1}{m_2^2}\right)H_{2(6)}(a)\right\} + \frac{D_{2(2)}}{2a^2}\right\} = 0, \tag{32}$$

$$\frac{m^2}{k^2}\left(1-k^2-\lambda^2\right)\left(\frac{\sigma_\infty}{\sigma_{ye}}\right)_{b(2)} + \frac{2}{\pi}\left\{\frac{m^3}{k}I_{1(5)} - \frac{m_2^3}{k_2}\left\{I_{2(6)} + \left(1-\frac{1}{k_2^2}\right)H_{2(6)}(b)\right\}\right. \tag{33}$$

$$+\frac{D_{2(2)}}{2a^2}\Bigg\} = 0,$$

$$\frac{m^2}{k^2}\lambda^2\left(\frac{\sigma_\infty}{\sigma_{ye}}\right)_{c(2)} - \frac{2}{\pi}\left\{\frac{m^3}{k}\left\{I_{1(5)} + \left(1-\frac{1}{k^2}\right)H_{1(5)}(c)\right\} - \frac{m_2^3}{k_2}I_{2(6)} + \frac{D_{2(2)}}{2a^2}\right\} = 0. \tag{34}$$

These non-linear equations enable us to study the behavior of yield zone lengths under the application of uniform stress distribution σ_∞ and variable yield stress distribution $\frac{t^s}{a^s}\sigma_{ye}$. However, it is almost impossible to write these equations as an explicit function of the applied load ratio. Therefore, a study is carried out to discuss these results numerically so that the results can be reported graphically.

5. Verification of analytical expressions

- SIFs calculated at the crack tips (a, b, and c) given in Eqs. (4–6) respectively, can be verified with the expressions given by Tada [17].
- SIFs calculated at the crack tips (a and b) given in Eqs. (17, 18), respectively, also be verified with the expressions given by [6] (as a limiting case) by taking $g_1 = g_2$ and $c = c_1 = h \to 0$.

6. Illustrations

In this section, the approximate length of yield zones at each crack tip is obtained numerically by using Eqs. (26–34). The yield zone length in this study is normalized with respective crack lengths and plotted against the applied load ratio $\frac{\sigma_\infty}{\sigma_{ye}}$ for different inter crack distances using the parameter $u = \frac{2c_1}{b_1+c_1}$. The parameter u denotes the positions of the cracks. Fictitious cracks R_1, R_2, and R_3 are situated are situated far away from each other when $u = 0.1, 0.2, 0.3$, etc, while the values $u = 0.9, 0.8, 0.7$ indicates closely positioned cracks.

6.1. Analysis for equal and symmetric straight cracks

6.1.1. At crack tips $\pm a$

A numerical illustrative study is presented in which the variations between normalized yield zone lengths $\frac{a-a_1}{a_1-b_1}$ and applied load ratio $\left(\frac{\sigma_\infty}{\sigma_{ye}}\right)$ have been plotted at crack tip a for three stress profiles as shown in Figures 6–8. Further, the results for three stress profiles are compared when three pairs of cracks are situated close to each other, $u = 0.6, 0.7, 0.8, 0.9$, as shown in Figure 9.

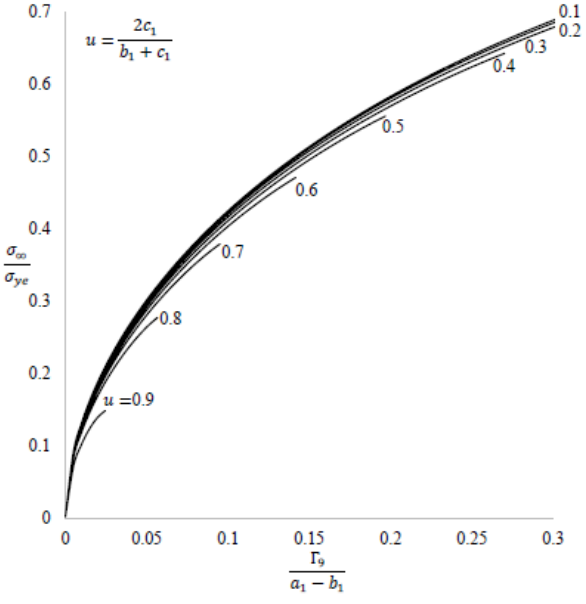


Fig. 6. Variation between normalized yield zone and load ratio for yield stress $\pm a_1$.

Figure 6 depicts the behavior of yield zone length under general yielding conditions. It is observed from the figure that as the applied load ratio increases, yield zone length at outer crack tip a_1 increases. But when cracks are situated far away from each other (for small values of u) insignificant difference is seen in the load-carrying capacity of the plate due to non-interacting cracks.

The influence of linear and quadratically varying stress distribution on the yield zones are depicted in Figures 7 and 8. It is seen from these figures that the load-carrying capacity of the sheet containing three pairs of collinear straight cracks

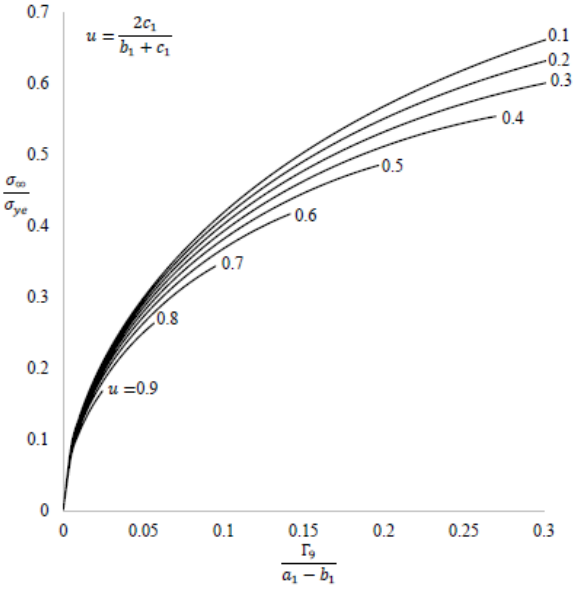


Fig. 7. Variation between normalized yield zone and load ratio for linearly varying yield stress $\pm a_1$.

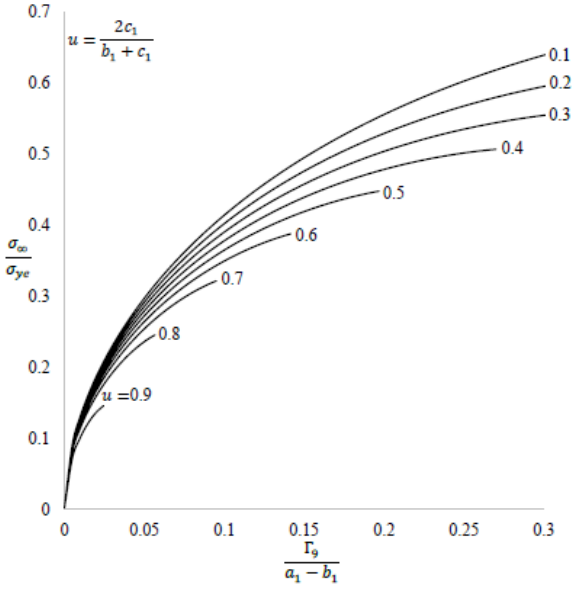


Fig. 8. Variation between normalized yield zone and load ratio for quadratically varying yield stress $\pm a_1$.

with unified yield zones at the crack tips, $\pm a_1$, is inferior as compared to constant yield stress distribution.

The significant difference in the load-carrying capacity of the plate can be observed in a comparative graph of all stress profiles, which is shown in Figure 9. It indicates that the structures may fail at a stress level that was well below the yield stress of the material, as discussed in [19].

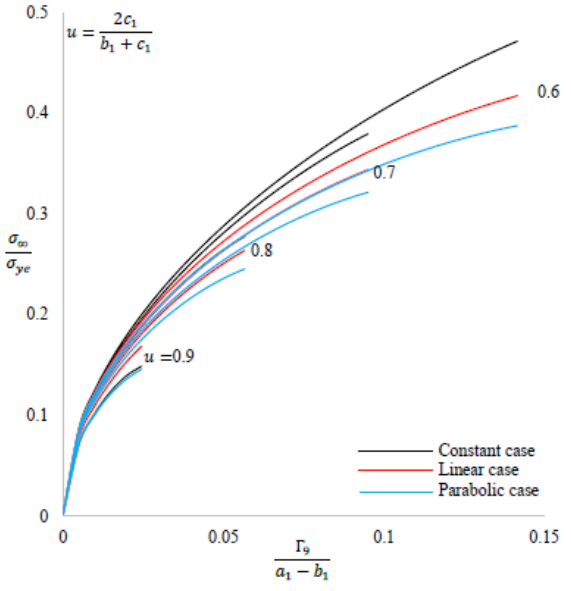


Fig. 9. Comparison between three stress profiles $\pm a_1$.

6.1.2. At crack tips $\pm b_1$

The same variations between normalized yield zone length $\frac{\Gamma_7}{a_1 - b_1}$ and load ratio $\frac{\sigma_\infty}{\sigma_{ye}}$ at crack tips, $\pm b_1$, have been plotted in Figures 10–12 for constant, linear, and quadratic yield stress distribution. It is seen from the figures that the plate can bear more load in case of constant yield stress distribution rather than variable stress distribution at the internal tips $\pm b_1$.

One insignificant effect of variable stress distribution on the load-bearing capacity of the plate is seen when the value of u will be small, due to non-interacting cracks. But, when cracks are closed to each other (for higher values of u) the yield zone length at crack tips $\pm b_1$ is affected significantly by the variable stress distribution. Hence, the crack tips $\pm b_1$ are much sensitive about the applied load ratio.

Figure 13 shows the effect of three stress profiles on the yield zone length. The load-bearing capacity of the plate is comparatively quite low when

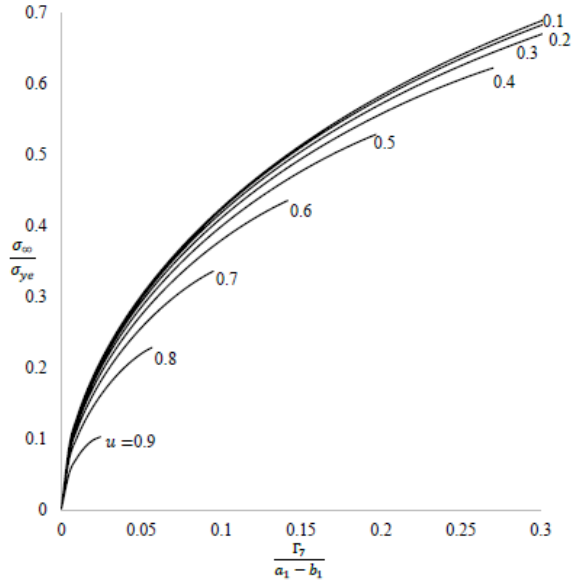


Fig. 10. Variation between normalized yield zone and load ratio for yield stress at $\pm b_1$.

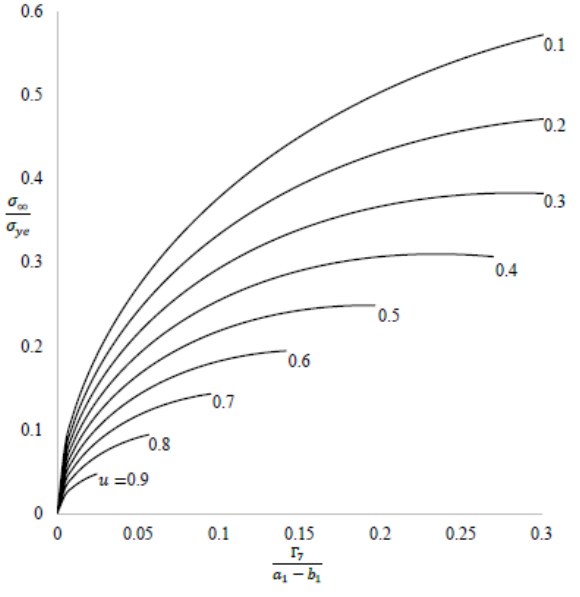


Fig. 11. Variation between normalized yield zone and load ratio for linearly varying yield stress at $\pm b_1$.

quadratic stress distribution is assumed to be acted on faces of the yield zones as cracks are situated close to each other as $u = 0.6, 0.7, 0.8, 0.9$.

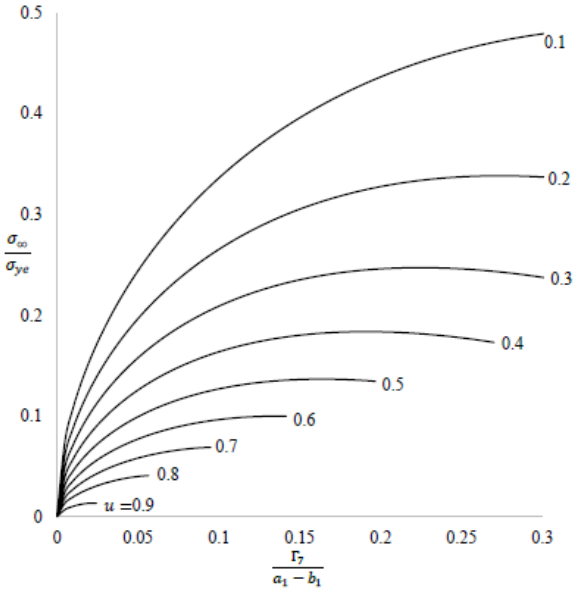


Fig. 12. Variation between normalized yield zone and load ratio for quadratically varying yield stress at $\pm b_1$.

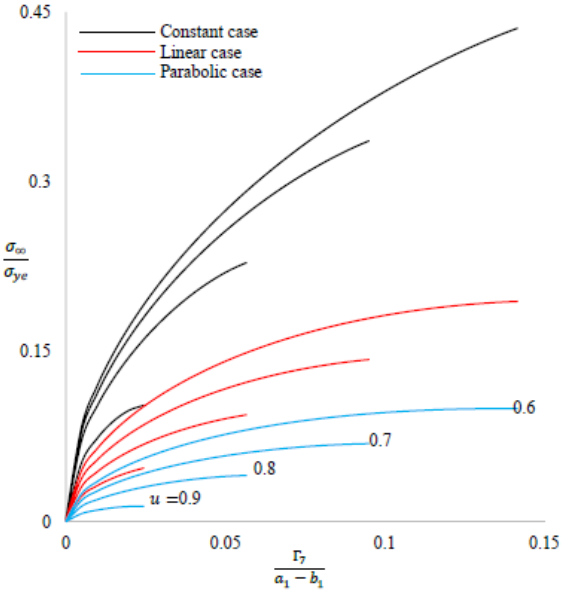


Fig. 13. Comparison between three stress profiles at $\pm b_1$.

6.1.3. At crack tips $\pm c$

Figures 9–11 show the behavior of applied stress ratio $\left(\frac{\sigma_\infty}{\sigma_{ye}}\right)_c$ with respect to normalized yield

zone length $\frac{\Gamma_6}{2c_1}$ at crack tips ($x = \pm c_1$) for constant, linear, and quadratically varying stress distribution.

According to the figure, the load-carrying capacity of the sheet in the presence of three pairs of collinear straight cracks with unified yield zones is more in case of under constant yield stresses while a very less load carrying capacity is seen in the case of under linear and quadratically varying yield stresses.

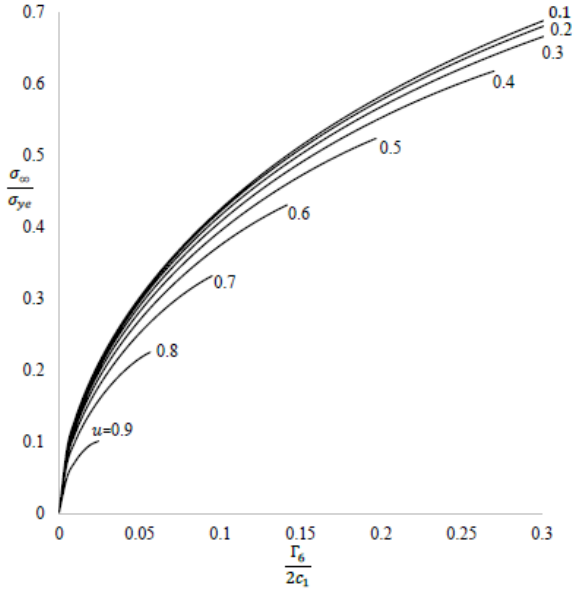


Fig. 14. Variation between normalized yield zone and load ratio for yield stress at $\pm c_1$.

Moreover, the load-carrying capacity of the sheet at the crack tips $\pm c_1$ is quite low in comparison to that of at crack tips a_1 and b_1 when rims of yield zones are subjected to variable yield stress distribution.

Figure 17 depicts the behavior of yield zones length at crack tips $\pm c_1$ when cracks are situated in close vicinity.

6.1.4. Analysis for unequal and symmetric straight cracks

In this section, the interaction between small and big cracks is investigated when central pair of cracks with unified yield zones of length $2c$ is taken which is five times larger than the outer pairs of

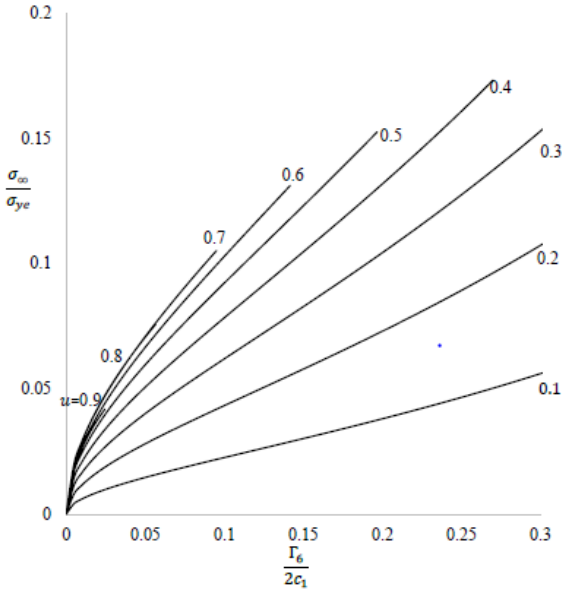


Fig. 15. Variation between normalized yield zone and load ratio for linearly varying yield stress at $\pm c_1$.

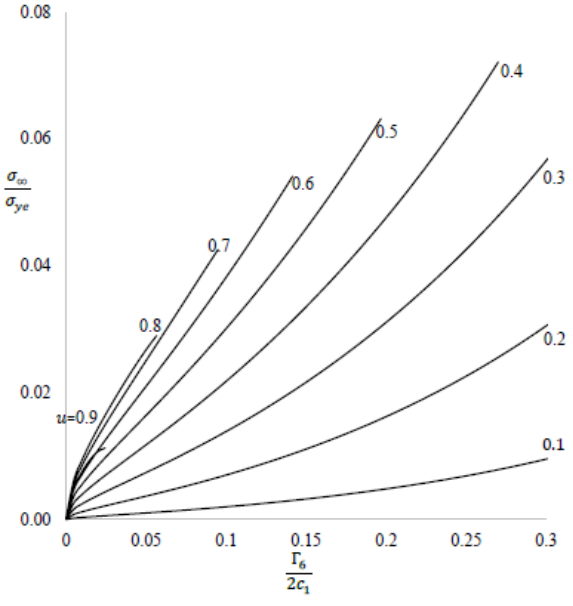


Fig. 16. Variation between normalized yield zone and load ratio for quadratically varying yield stress at $\pm c_1$.

cracks. A similar variation is plotted at each crack tip.

Figure 18 shows the variation of applied load

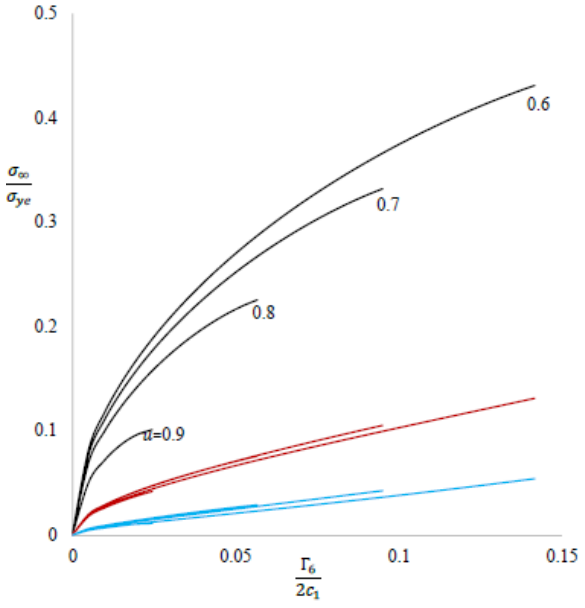


Fig. 17. Comparison between three stress profiles at $\pm c_1$.

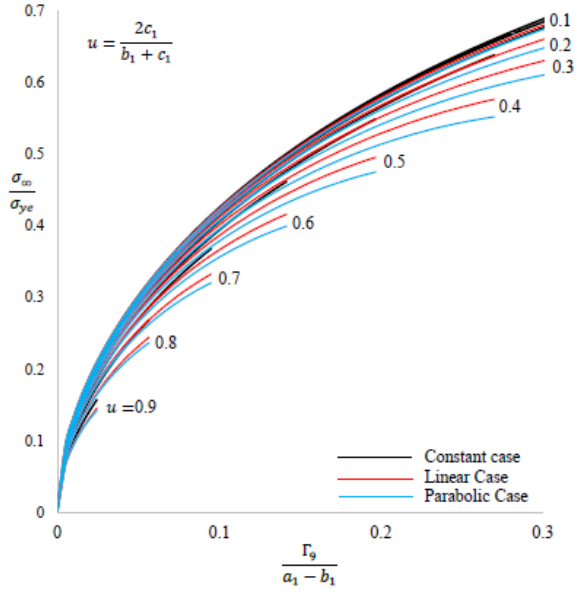


Fig. 18. Variation between $\frac{\Gamma_6}{a_1-b_1}$ and $\left(\frac{\sigma_\infty}{\sigma_{ye}}\right)_a$.

ratio $\left(\frac{\sigma_\infty}{\sigma_{ye}}\right)_a$ with respect to normalized plastic zones for different values of u at the crack tip a_1 for three stress profiles. It is noticed from the Figure 18 that the yield zone length increases as the applied stress increases when three stress profiles are considered. However, the load-carrying capacity of the plate at crack tip a_1 is very low in case of parabolically varying stress distribution within the plastic enclaves when cracks are assumed to be placed in closed proximity.

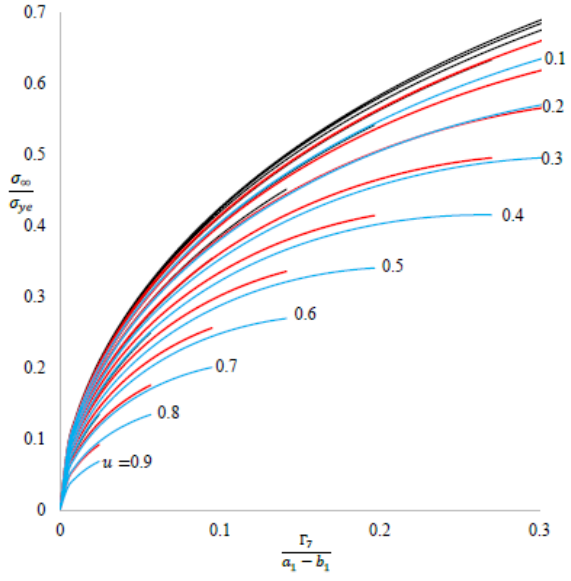


Fig. 19. Variation between $\frac{\Gamma_6}{a_1-b_1}$ and $\left(\frac{\sigma_\infty}{\sigma_{ye}}\right)_b$.

Figure 19 shows the effect of normalized yield zone $\frac{\Gamma_6}{a_1-b_1}$ ($\Gamma_6 = |b_1 - b|$) on the applied stress ratio $\left(\frac{\sigma_\infty}{\sigma_{ye}}\right)_b$ at the crack tip b_1. It has been observed from Figure 14 that yield zones developed at the crack tip b_1 are much larger than the yield zone at crack tip a_1 when the cracks are close to each other, i.e., $u = 0.6, 0.7, 0.8, 0.9$. Further, for a fixed yield zone size, the load carrying capacity of the plate at the crack tip b_1 is less in this configuration in comparison to that in case of three pairs of equal cracks with unified yield zones since bigger interior cracks make a significant impression on outer pairs of cracks.

The variations between yield zone ratio $\frac{\Gamma_5}{2c_1}$ ($\Gamma_5 = |c - c_1|$) and load ratio $\left(\frac{\sigma_\infty}{\sigma_{ye}}\right)_c$ at crack tips c_1 is plotted in Figure 20. Low bearing capacity of the plate as far as to crack tip c_1 is a big concern in case of parabolically varying yield stress distribution when cracks are placed far away from each

other due to small value of $\frac{t^2}{a^2}\sigma_{ye}$. In the case of constant yield stress distribution, the load-carrying capacity of the plate is the same for all values of u as the big central pair of cracks has an insignificant impression of the presence of small side pairs of cracks.

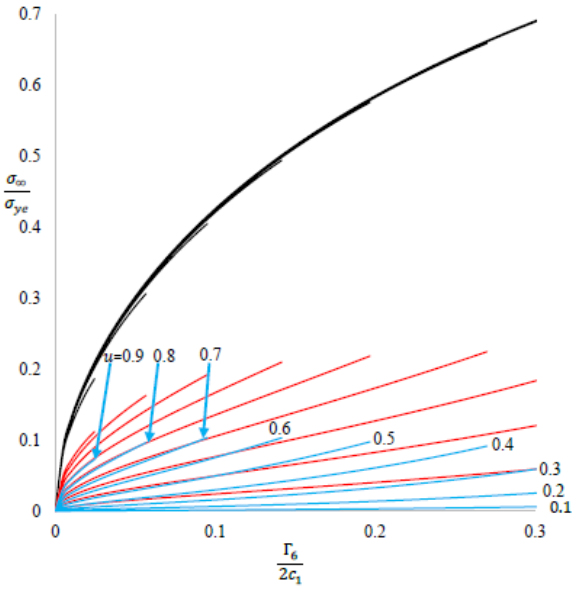


Fig. 20. Variation between $\frac{\Gamma_5}{2c_1}$ and $(\frac{\sigma_\infty}{\sigma_{ye}})_c$.

6.1.5. Comparison with results of three equal straight cracks

In this section, the results obtained for the configuration shown in Figure 1 are compared with the results of three equal straight cracks given in [10]. Here, the yield zone lengths are normalized with the zone length, $r_j = x\left[\sec\left(\frac{\pi\sigma_\infty}{2\sigma_{ye}}\right) - 1\right]$, of single Dugdale's crack of equivalent configuration of length $2x$, where $j = A, B, C$ and x is the corresponding crack tip.

Figure 21 shows the variation between applied load ratio $\left(\frac{\sigma_\infty}{\sigma_{ye}}\right)_a$ and yield zone ratio $\frac{\Gamma_8}{r_A}$ for different values of u where r_A is the length of yield zone developed in case of single Dugdale crack of length $2a_1$. It is noticed from the Figure 21 that the entire configuration in both the cases behaves like a single crack when these cracks are situated far away from each other, i. e., $u = 0.1, 0.2$. But when these cracks are assumed to be situated close to each other the load-bearing capacity is much higher in the case of three pairs of collinear straight cracks with unified yield zones as compared to three equal straight cracks.

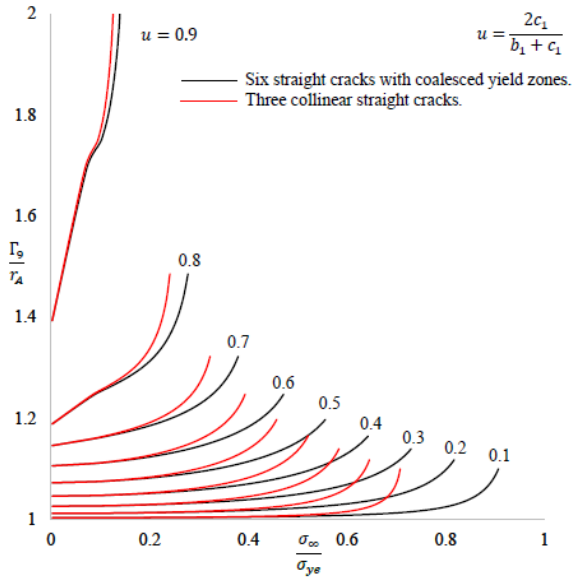


Fig. 21. Variation between $\frac{\Gamma_6}{r_B}$ and $\left(\frac{\sigma_\infty}{\sigma_{ye}}\right)_a$.

Effect of the length of unified yield zones on the load-carrying capacity of the sheet at the crack tips $x = \pm b_1$ is plotted in Figure 22. Here, the results of yield zone length are normalized with the yield zone length in case of a single central Dugdale crack of length $2b_1$. It has been observed from the Figure 16 that the load-carrying capacity of the sheet in the case of three pairs of collinear straight cracks with unified yield zones is higher in comparison to that in the case of three collinear straight cracks. Therefore, the plate can bear more load in case of multiple cracks with coalesced yield zones.

Finally, we would like to investigate the behavior of yield zone ratio $\frac{\Gamma_5}{r_C}$ $(\Gamma_5 = |c - c_1|)$ with respect to load ratio $\left(\frac{\sigma_\infty}{\sigma_{ye}}\right)$ at crack tips $x = \pm c_1$, which is plotted in Figure 23. It is observed that the yield zone lengths are approximately the same in the case of three pairs of collinear straight cracks with unified yield zones and three collinear straight cracks at crack tips $x = \pm c_1$ when the applied load

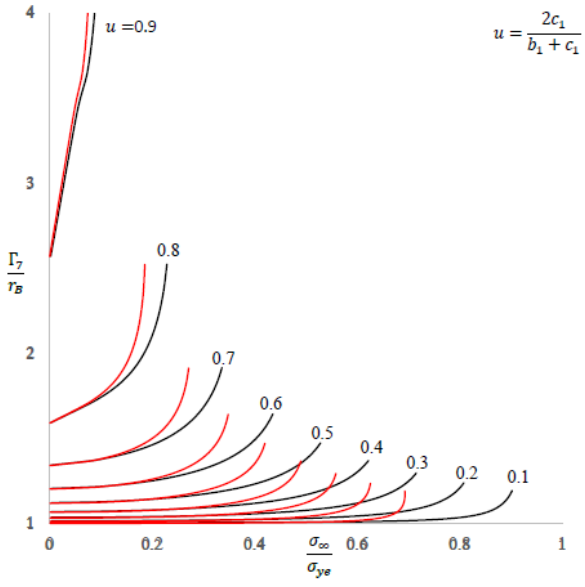


Fig. 22. Variation between $\frac{\Gamma_6}{r_B}$ and $\left(\frac{\sigma_\infty}{\sigma_{ye}}\right)_b$.

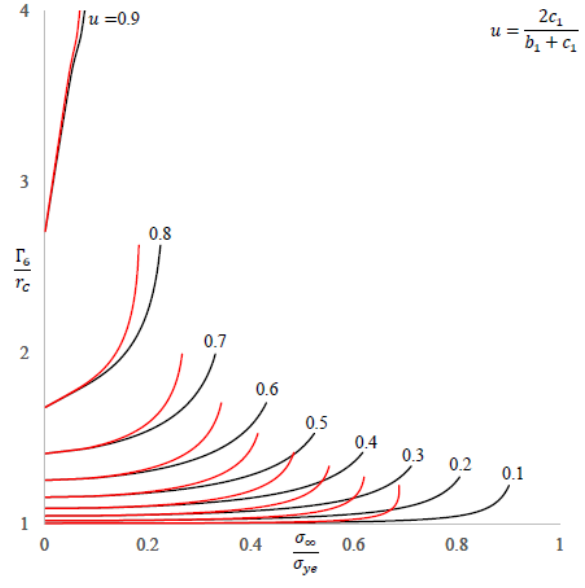


Fig. 23. Variation between $\frac{\Gamma_5}{r_C}$ and $\left(\frac{\sigma_\infty}{\sigma_{ye}}\right)_c$.

is small and cracks are situated far away from each other. However, a large yield zone is seen in the case of three collinear straight cracks when applied load is approximately the same as the yield stress of the material.

7. Conclusion and discussion

In this paper, a complicated practical case of the Multi-site damage (MSD) problem of three pairs of symmetrical collinear straight cracks with coalesced yield zones in an infinite sheet is studied using a modified Dugdale-Barenblatt (DB) strip yield model. Closed-form expressions for important fracture parameters like SIFs and yield zone length are obtained using the complex variable method. The formulae (26–34) are exact analytical expressions, which provide a useful theoretical base for the numerical study of yield zone length and load-carrying capacity of the plate. Since the effect of interaction is strongly dependent on the distance between cracks, therefore results for $u = 0.7, 0.8, 0.9$ are the main results which are presented in this paper.

Based on the numerical study presented in Section 6, some observations are made. It is noticed that when cracks are situated far away from each other (e. g., $u = 0.1, 0.2, 0.3$) and applied stress is small when compared to yield stress, the developed yield zones at each external tips of three pairs of collinear straight cracks with coalesced yield zones behave similar to the case of three collinear straight cracks. But when cracks are situated close to each other, the length of inner yield zones is much bigger than the outer yield zones. Large yield zone length is observed in the case of quadratically varying yield stresses when compared to linearly varying loading conditions at all crack tips.

Conflict of interests

The author declares that there is no conflict of interest.

References

[1] Dugdale DS. Yielding of steel sheets containing slits. *J Mech Phys Solids*. 1960;8(2):100–4.

[2] Harrop LP. Application of a modified Dugdale model to the *k* vs *cod* relation. *Eng Fract Mech*. 1978;10(4):807–16.

[3] Kanninen MF. A solution for a Dugdale crack subjected to a linearly varying tensile loading. *Int J Eng Sci*. 1970;8(1):85–95.

[4] Neimitz A. Analysis of the crack motion with varying velocity according to the Dugdale-Panasyuk model. *Eng Fract Mech*. 1991;39(2):329–38.

[5] Theocaris PS. Dugdale models for two collinear unequal cracks. *Eng Fract Mech*. 1983;18(3):545–59.

[6] Collins RA, Cartwright DJ. An analytical solution for two equal-length collinear strip yield cracks. *Eng Fract Mech* 2001;68(7):915–24.
[7] Bhargava RR, Hasan S. Crack opening displacement for two unequal straight cracks with coalesced plastic zones – A modified Dugdale model. *Appl Math Modell*. 2011;35(8):3788–96.
[8] Xu W, Wu XR, Wang H. Weight functions and strip yield solution for two equal-length collinear cracks in an infinite sheet. *Eng Fract Mech*. 2011;78(11):2356–68.
[9] Wu KC, Huang SM, Dugdale model for an expanding crack under shear stress. *Eng Fract Mech*. 2013;104:198–207.
[10] Hasan S, Akhtar N. Dugdale model for three equal collinear straight cracks: an analytical approach. *Theor Appl Fract Mech*. 2015;78:40–50.
[11] Hasan S, Akhtar N. Mathematical model for three equal collinear straight cracks: a modified Dugdale approach. *Strength Fract Complex* Int J. 2015;9(3):211–32.
[12] Xu W, Wu XR. Weight functions and strip-yield model analysis for three collinear cracks. *Eng Fract Mech*. 2012;85:73–87.
[13] Kim JH, Lee SB. Fatigue crack opening stress based on the strip-yield model. *Theor Appl Fract Mech*. 2000;34(1):73–84.
[14] Feng XQ, Gross D. On the coalescence of collinear cracks in quasi-brittle materials. *Eng Fract Mech*. 2000;65(5):511–24.
[15] Bhargava RR, Hasan S. Crack-tip-opening displacement for four symmetrically situated cracks with coalesced interior yield zones. *Appl Math Modell*. 2012;36(11):5741–9.
[16] Akhtar N, Hasan S. Assessment of the interaction between three collinear unequal straight cracks with unified yield zones. *AIMS Mater Sci*. 2017;4(2)302–16.
[17] Tada H, Paris PC, Erwin GR. *The Stress Analysis of Cracks Handbook*, 3rd ed. New York: ASME Press; 2000.
[18] Byrd P, Friedman M. *Handbook of Elliptical Integrals for Engineers and Scientist*. Springer-Verlag, New York Heidelberg Berlin; 1971. `https://link.springer.com/book/10.1007/978-3-642-65138-0`.
[19] Gdoutos EE. *Fracture Mechanics: An Introduction,* 2nd ed. Springer, Netherlands; 2005.
[20] Muskhelishvili NI. *Some Basic Problems of Mathematical Theory of Elasticity*. In: Noordhoff P, editor. Leiden; 1963.
[21] Cherenapov GP. *Mechanics of Brittle Fracture.* Nauka Press, Moskow; 1974.

Appendix A: basic mathematical equations

In two-dimensional theory of elasticity, the components of stresses X_x, Y_y, X_y may be expressed in terms of two complex potential functions $\Phi(z), \Omega(z)$ as

$$X_x + Y_y = 2\left[\Phi(z) + \overline{\Phi(z)}\right], \tag{35}$$

$$Y_y - iX_y = \Phi(z) + \Omega(\bar{z}) + (z-\bar{z})\overline{\Phi'(z)}, \tag{36}$$

where bar (line) over the function or variable denotes its complex conjugate.

Consider a homogenous isotropic infinite elastic-perfectly plastic plate weakened by n collinear straight cuts (i=1, 2, 3,, n) along ox-axis. Let $X_y^{\pm}, Y_y^{\pm}$ be the components of stresses acting over the rims of the cracks. Superscript $(+)$ and $(-)$ denoting the values of stress components on the upper and lower rims of the cracks.

Eqs. (35, 36) may be converted into two problems of linear relationship

$$\Phi^+(t) + \Omega^-(t) = Y_y^+ - iX_y^+, \tag{37}$$

$$\Phi^-(t) + \Omega^+(t) = Y_y^- - iX_y^-. \tag{38}$$

under the assumption $\lim_{y\to 0} y\Phi'(t+iy) = 0$.

The general solution of the boundary value problems given in Eqs. (37, 38) may be written using Plemelj formula [20] as:

$$\Phi(z) + \Omega(z) = \frac{1}{\pi i \chi(z)} \int_L \frac{\chi(t)\, p(t)\, dt}{t-z} + \frac{2P_n(z)}{\chi(z)} \tag{39}$$

$$\Phi(z) - \Omega(z) = \frac{1}{\pi i} \int_L \frac{q(t)\, dt}{t-z} - \overline{\Gamma'}, \tag{40}$$

where

$$p(t) = \frac{1}{2}\left[Y_y^+ + Y_y^-\right] - \frac{i}{2}\left[X_y^+ + X_y^-\right],$$
$$q(t) = \frac{1}{2}\left[Y_y^+ - Y_y^-\right] - \frac{i}{2}\left[X_y^+ - X_y^-\right],$$

$$\chi(z)=\prod_{k=1}^{n}\sqrt{z-a_k}\sqrt{z-b_k},$$
$$P_n(z)=D_0z^n+D_1z^{n-1}+D_2z^{n-2}+\ldots,$$

a_k, b_k denote the end points of k^{th} crack.

Constants $D_i\,(i=0,1,2,..,n)$ shown in $P_n(z)$ are evaluated using the loading conditions at the infinite boundary of the plate and single-valued condition of displacement around the rims of the cracks or cuts,

$$\begin{aligned}&2(\kappa+1)\int_{L_i}\frac{P_n(t)}{\chi(t)}dt\\&+\kappa\int_{L_i}\left[\Phi_0^+(t)-\Phi_0^-(t)\right]dt\\&+\int_{L_i}\left[\Omega_0^+(t)-\Omega_0^-(t)\right]dt=0.\end{aligned}\tag{41}$$

where

$$\begin{aligned}\Phi_0(z)=&\frac{1}{2\pi i\chi(z)}\int_{\bigcup_{i=1}^{n}L_i}\frac{\chi^+(t)\,p(t)}{t-z}dt\\&+\frac{1}{2\pi i}\int_{\bigcup_{i=1}^{n}L_i}\frac{q(t)}{t-z}dt,\end{aligned}\tag{42}$$

$$\begin{aligned}\Omega_0(z)=&\frac{1}{2\pi i\chi(z)}\int_{\bigcup_{i=1}^{n}L_i}\frac{\chi^+(t)\,p(t)}{t-z}dt\\&-\frac{1}{2\pi i}\int_{\bigcup_{i=1}^{n}L_i}\frac{q(t)}{t-z}dt,\end{aligned}\tag{43}$$

Stress intensity factor

Mode-I type stress intensity factor at each crack tip $z=z_1$ is evaluated using the formula given in [21],

$$K_I=2\sqrt{2\pi}\lim_{z\to z_1}\sqrt{z-z_1}\Phi(z).\tag{44}$$

Note: The mathematical formulations given above are taken form Muskhelishvili [20] to make the paper self-sufficient. All the integrals are solved in the form of elliptic integrals whose definitions are given in [18].

Appendix B: used mathematical expressions

The expressions of terms used in the paper are given in this section:

$$\begin{aligned}J_{1i}=&\,j_i(\phi(a_1),m,k)-j_i(\phi(b_1),m,k)\\&+j_i(\phi(b),m,k)+j_i(\phi(g_2),m,k)\\&-j_i(\phi(g_1),m,k),\end{aligned}$$

$$\begin{aligned}J_{2i}=&\,j_i(\vartheta(c_1),m_2,k_2)-j_i(\vartheta(c),m_2,k_2)\\&+j_i(\vartheta(0),m_2,k_2)-j_i(\vartheta(h),m_2,k_2),\end{aligned}$$

$$\begin{aligned}I_{1(\mathrm{i})}=&\,\ell_i(\phi(a_1),m,k)-\ell_i(\phi(b_1),m,k)\\&+\ell_i(\phi(b),m,k)+\ell_i(\phi(g_2),m,k)\\&-\ell_i(\phi(g_1),m,k),\end{aligned}$$

$$\begin{aligned}I_{2(\mathrm{i})}=&\,\ell_i(\vartheta(c_1),m_2,k_2)-\ell_i(\vartheta(c),m_2,k_2)\\&+\ell_i(\vartheta(0),m_2,k_2)-\ell_i(\vartheta(h),m_2,k_2),\end{aligned}$$

$$\begin{aligned}H_{1(\mathrm{i})}(z)=&\,h_i(\phi(a_1),m,k,n(z))\\&-h_i(\phi(b_1),m,k,n(z))\\&+h_i(\phi(b),m,k,n(z))\\&+h_i(\phi(g_2),m,k,n(z))\\&-h_i(\phi(g_1),m,k,n(z)),\end{aligned}$$

$$\begin{aligned}H_{2(\mathrm{i})}(z)=&\,h_i(\vartheta(c_1),m_2,k_2,n_2(z))\\&-h_i(\vartheta(c),m_2,k_2,n_2(z))\\&+h_i(\vartheta(0),m_2,k_2,n_2(z))\\&-h_i(\vartheta(h),m_2,k_2,n_2(z)),\end{aligned}$$

$$\begin{aligned}\nu_i=&\,w_i(\xi(c_1),k_2,k_1)+w_i(\xi(0),k_2,k_1)\\&-w_i(\xi(h),k_2,k_1),\end{aligned}$$

$$\begin{aligned}W_i=&\,w_i(\psi(c_1),m,k)-w_i(\psi(h),m,k)\\&+w_i(\psi(0),m,k),\end{aligned}$$

$$\tau(\theta,k)=E(\theta,k)-\lambda^2F(\theta,k),$$

$$\rho(\theta,k) = E(\theta,k) - \tan\theta\sqrt{1-k^2\sin^2\theta},$$

$$M(\theta,m,k) = \frac{1-k^2}{k^2\sqrt{1-m^2}}\Pi\left(\theta_1(\theta,m),k^2,k_1\right) + \frac{1}{mk}\tan^{-1}\left(\frac{m\,k\,\sin\theta\,\cos\theta}{\sqrt{1-m^2\sin^2\theta}\sqrt{1-k^2\sin^2\theta}}\right),$$

$$S(\theta,m,k) = \frac{m^2\sin 2\theta\sqrt{1-k^2\sin^2\theta}}{2\left(1-m^2\sin^2\theta\right)},$$

$$\Lambda(\theta,m,k) = \frac{\sin 2\theta\sqrt{1-k^2\sin^2\theta}}{4\sqrt{1-m^2\sin^2\theta}},$$

$$\theta_1(\theta,m) = \tan^{-1}\left(\tan(\theta)\sqrt{1-m^2}\right),$$

$$\theta_2(\theta,m) = \tan^{-1}\left(\frac{m\cos\theta}{\sqrt{1-m^2}}\right),$$

$$\theta_3(\theta,m) = \tan^{-1}\left(\frac{\sqrt{1-m^2}}{m\cos\theta}\right),$$

$$\sin\vartheta(t) = \frac{t}{c},\quad k_2 = \frac{c}{b},\quad m_2 = \frac{c}{a},\quad n_2(t) = \frac{c}{t},$$

$$\sin\psi(t) = \sqrt{\frac{c^2-t^2}{b^2-t^2}},$$

$$\sin\varphi(t) = \sqrt{\frac{(t^2-b^2)(a^2-c^2)}{(t^2-c^2)(a^2-b^2)}},$$

$$\sin\xi(t) = \sqrt{\frac{b^2(c^2-t^2)}{c^2(b^2-t^2)}},$$

$$\sin\phi(t) = \sqrt{\frac{a^2-t^2}{a^2-b^2}},$$

$$k = \sqrt{\frac{a^2-b^2}{a^2-c^2}},\quad m = \sqrt{\frac{a^2-b^2}{a^2}},$$

$$n(t) = \sqrt{\frac{a^2-b^2}{a^2-t^2}},\quad k_1 = \sqrt{\frac{(a^2-b^2)c^2}{(a^2-c^2)b^2}},$$

$$\ell_1(\theta,p,q) = \frac{1}{p^2}\left(q^2M(\theta,p,q) - \ell_2(\theta,p,q)\right),$$

$$\ell_2(\theta,p,q) = \frac{q^2+p^2-p^2q^2}{2}M(\theta,p,q) + p^2\Lambda(\theta,p,q) + \frac{\sqrt{1-p^2}}{2}E(\theta_1(\theta,p),q_1) - \frac{(1-q^2)p^2}{2q^2\sqrt{1-p^2}}F(\theta_1(\theta,p),q_1),$$

$$\ell_3(\theta,p,q) = \frac{1}{3q^2}\Big[\left(1-q^2\right)F(\theta,q) + \left(2q^2-1\right)E(\theta,q) - 2q^2\Lambda(\theta,0,q)\Big],$$

$$\ell_4(\theta,p,q) = \frac{\left(p^2+q^2-2p^2q^2\right)\sqrt{1-p^2}}{3p^2q}\cdot E(\theta_2(\theta,q),q_2) - \left(\frac{2p^2\left(1-q^2\right)+q^2\left(1-p^2\sin^2\theta\right)}{3p^2}\right)\cdot\frac{2\Lambda(\theta,q,p)}{\sin\theta} - \frac{2\left(1-q^2\right)\sqrt{1-p^2}}{3q}\cdot F(\theta_2(\theta,q),q_2),$$

$$\ell_5(\theta,p,q) = \ell_6(\theta,p,q) = j\ell(\theta,p,q) - \frac{\left(p^2+q^2-3p^2q^2\right)}{4p^2q^2}\ell_2(\theta,p,q),$$

$$j_1(\theta,p,q) = \frac{1}{p^2}\left(\ell_2(\theta,p,q)\right.$$

$$- E(\theta,q)\sqrt{1-p^2\sin^2\theta}\Bigg),$$

$$j_2(\theta,p,q) = jh(\theta,p,q) - \frac{\sqrt{1-p^2\sin^2\theta}}{p^2}F(\theta,q),$$

$$j_3(\theta,p,q) = \frac{\Lambda(\theta,0,q)}{3} - \frac{1-q^2}{6q^2}F(\theta,q) + \left(\frac{2-q^2}{3q^2} - \frac{1-q^2\sin^2\theta}{2q^2}\right)E(\theta,q),$$

$$j_4(\theta,p,q) = \frac{E(\theta,q)}{2q^2} - \frac{1-q^2\sin^2\theta}{2q^2}F(\theta,q),$$

$$j_5(\theta,p,q) = \frac{\left(5q^2+p^2-3p^2q^2\right)}{12p^2q^2}\ell_2(\theta,p,q) - j\ell(\theta,p,q) - \frac{(1-p^2\sin^2\theta)^{\frac{3}{2}}}{3p^2}E(\theta,q),$$

$$j_6(\theta,p,q) = \frac{1}{3q^2}\Bigg(\ell_2(\theta,p,q) + \left(q^2-p^2\right)jh(\theta,p,q) - \frac{q^2(1-p^2\sin^2\theta)^{\frac{3}{2}}}{p^2}F(\theta,q)\Bigg),$$

$$h_1(\theta,p,q,r) = \frac{1}{r^2-p^2}\Big(h_2(\theta,p,q,r) - q^2r^2M(\theta,p,q)\Big),$$

$$h_2(\theta,p,q,r) = p^2q^2jh(\theta,p,q) + \frac{r^2-q^2}{\sqrt{1-p^2}}\Pi\left(\theta_1(\theta,p),r_1^2,q_1\right),$$

$$h_3(\theta,p,q,r) = \frac{q^2}{r^2}F(\theta,q) - E(\theta,q) + \left(1-\frac{q^2}{r^2}\right)\Pi\left(\theta,r^2,q\right),$$

$$h_4(\theta,p,q,r) = -\frac{2p^2}{\sin z}\Lambda(\theta,p,q) - q\sqrt{1-p^2}\Big\{E\left(\theta_3(\theta,p),q_2\right) + F\left(\theta_3(\theta,p),q_2\right)\Big\} + \frac{p^2\left(r^2-q^2\right)}{qr^2\sqrt{1-p^2}}\Pi\left(\theta_3(\theta,p),r_2^2,q_2\right),$$

$$h_5(\theta,p,q,r) = h_6(\theta,p,q,r) = \frac{h_2(\theta,p,q,r)}{r^2} - \ell_2(\theta,p,q),$$

$$w_1(\theta,p,q) = \frac{b}{2}\Big[E(\theta,q) - \left(1+k^2-2q^2\right)F(\theta,q) - \left(2q^2-p^2-k^2\right)\Pi\left(\theta,p^2,q\right) - S(\theta,p,q)\Big],$$

$$w_2(\theta,p,q) = b\Big[E(\theta,q) + k^2\left(p^2-1\right)F(\theta,q) + \left(p^2-1\right)\left(1-k^2\right)\Pi\left(\theta,p^2,q\right)\Big],$$

$$w_3(\theta,p,q) = b\Big[F(\theta,q) + \left(p^2-1\right)\Pi\left(\theta,p^2,q\right)\Big],$$

$$w_4(\theta,p,q) = -\frac{\left(b^2-c^2\right)^2}{b}\Big[k^2\Pi\left(\theta,p^2,q\right) - \left(2k^2-1\right)V_2(\theta,p,q) - \left(1-k^2\right)V_3(\theta,p,q)\Big],$$

$$w_5(\theta,p,q) = -\frac{a^2m^2b}{2k^2}\Big[E(\theta,q) - \left(k^2+1\right)F(\theta,q) - \left(p^2-k^2\right)\Pi\left(\theta,p^2,q\right) - S(\theta,p,q)\Big],$$

$$w_6(\theta,p,q) = \frac{a^2p^2}{3q^2}\Bigg[\left(1-2q^2\right)\rho(\theta,q) + \left(q^2-1\right)F(\theta,q) + \frac{2\left(1-q^2\right)}{\cos^4 z}\Lambda(\theta,p,q)\Bigg],$$

$$w_7(\theta,p,q)=\frac{b^2}{2}\Big(E(\theta,q)-\left(1-k_2^2\right)\left(F(\theta,q)-\rho(\theta,q)\right)\Big),$$

$$w_8(\theta,p,q)=c^2F(\theta,q)+\frac{a^2p^2}{q^2}\rho(\theta,q),$$

$$V_2(z,p,q)=\frac{1}{2\left(p^2-1\right)\left(q^2-p^2\right)}\cdot\begin{bmatrix}p^2E(z,q)+\left(q^2-p^2\right)F(z,q)+\\ \left(2p^2q^2+2p^2-p^4-3q^2\right)\\ \Pi\left(z,p^2,q\right)\\ -p^2S(z,p,q)\end{bmatrix},$$

$$V_3(z,p,q)=\frac{1}{4\left(1-p^2\right)\left(q^2-p^2\right)}\cdot\begin{bmatrix}q^2F(z,q)+\\ 2\left(p^2q^2+p^2-3q^2\right)\Pi\left(z,p^2,q\right)+\\ 3\left(p^4-2p^2q^2-2p^2+3q^2\right)\\ V_2(z,p,q)+\frac{p^2S(z,p,q)}{1-p^2\sin^2z}\end{bmatrix},$$

$$j\ell(\theta,p,q)=\frac{q^4+p^4-p^2q^2\left(p^2+q^2\right)}{4p^2q^2}M(\theta,p,q)+\frac{\left(q^2-p^2\right)\left(1-q^2\right)}{4q^4\sqrt{1-p^2}}F\left(\theta_1(\theta,p),q_1\right)-\frac{1-p^2\sin^2\theta}{2}\Lambda(\theta,q,p),$$

$$jh(\theta,p,q)=M(\theta,p,q)+\frac{q^2-p^2}{q^2p^2\sqrt{1-p^2}}F\left(\theta_1(\theta,p),q_1\right),$$

$$q_1=\sqrt{\frac{q^2-p^2}{1-p^2}},\quad r_1=\sqrt{\frac{r^2-p^2}{1-p^2}},\quad q_2=\frac{q_1}{q},$$

$$r_2=\frac{r_1}{r}.$$

Received 2021-06-21
Accepted 2021-08-16